


PRECIPITATION-RELATED INCREASE EVENTS OF THE ELECTROMAGNETIC COMPONENT OF SECONDARY COSMIC RAYS: SPECTRAL ANALYSIS

Yu.V. Balabin 
Polar Geophysical Institute,
Apatity, Russia, balabin@pgia.ru

A.V. Germanenko 
Polar Geophysical Institute,
Apatity, Russia, alex.germanenko@gmail.com

B.B. Gvozdevsky 
Polar Geophysical Institute,

Apatity, Russia, gvozdevsky@pgia.ru

E.A. Mauricev 
Polar Geophysical Institute,
Apatity, Russia, maurchev1987@gmail.com

E.A. Michalko 
Polar Geophysical Institute,
Apatity, Russia, mikhalko@pgia.ru

Abstract. We report the measurement results of differential spectra of electromagnetic radiation in the range 0.1–4 MeV, which occurs in the atmosphere as a component of secondary cosmic rays. Spectral monitoring was performed using a spectrometer based on the Nai (TL) crystal in 2022–2023. The main purpose of the measurements was to determine spectral characteristics of the electromagnetic radiation during increase events, when the electromagnetic radiation flux from the atmosphere rises by tens of percent with respect to the background level. From a thorough analysis of the spectra of many dozens of events, we have drawn a conclusion that although the lines of natural radionuclides are

present on the spectra and contribute their share, their total contribution to the increase events is ~0.1 of the total energy supplied during an increase. We unambiguously conclude that the effect of increasing electromagnetic radiation during precipitation is not due to the presence of radionuclides in precipitation.

Keywords: secondary cosmic rays, electromagnetic radiation, scintillation detector, differential spectrum, radionuclides, increase.

INTRODUCTION

Cosmic ray detectors located on Earth's surface detect secondary cosmic rays (SCRs) formed by the interaction between primary cosmic rays and air atomic nuclei. The cosmic-ray particles first interact in the upper atmospheric layers up to ~10–15 km [Hayakawa, 1974]; then SCRs propagate deep into the atmosphere. They consist of several components [Murzin, 1988]. The SCR nucleon component is detected by neutron monitors; muon telescopes are sensitive to the charged component of SCRs [Dorman, 1975]. The SCR high-energy (hundreds of MeV) electromagnetic component produces cascades of light particles [Ivanenko, 1972]. The SCR low-energy (<100 MeV) electromagnetic component is strongly absorbed and dispersed by the atmosphere. For example, the free path of quanta with energies of a few of MeV does not exceed several hundred meters [Grigoriev, Melikhov, 1991]; therefore, all such quanta recorded by a ground instrument were formed at altitudes no higher than 1–2 km [Murzin, 1988]. This means that SCRs produce new quanta of electromagnetic radiation throughout the atmosphere due to the decay of short-lived particles (muons, kaons, pions) and the bremsstrahlung radiation of light charged particles [Hayakawa, 1974; Murzin, 1988]. The SCR electromagnetic component (EMC) is of little use for studying cosmic rays since it is strongly influenced by the atmosphere [Dorman, 1972], but that is why it can be a good indicator of meteorological processes in the surface layer of the atmosphere.

1. MONITORING OF ELECTROMAGNETIC RADIATION FLUX

Since 2009, scientists of the Polar Geophysical Institute (PGI) at the cosmic ray station in Apatity have been monitoring electromagnetic radiation coming from the atmosphere. The monitoring is carried out using detectors based on NaI(Tl) scintillation crystals 65 mm in diameter and 20 mm in height, developed at PGI for measuring X-rays [Lazutin, 1979]. The detectors, calibrated against the Am-241 lines (27 and 61 keV), are housed in lead cups with walls 50 mm thick and have a field of view of ~150° in the form of a cone with the base oriented to the zenith. The detectors are located in a thermostabilized box in the attic of the building. Above the detectors is a total of 0.8 g/cm² of iron and ~2 g/cm² of wood (iron roof and boards), these values were used to calculate the absorption of radiation in the roof of the building [Grigoriev, Melikhov, 1991]. The detector efficiency was calculated using the RUSCOSMICS software package [Germanenko et al., 2019]; based on this, the energy range of the detector is taken to be 20–500 keV, although the crystal is capable of detecting radiation up to 1 MeV. The detectors have several integrated outputs, the most convenient and stable channel is >100 keV. The complex for measuring SCR fluxes is described in detail by Balabin et al. [2014].

After the start of observations, a precipitation-related increase in EMC was detected very soon. In what follows, for brevity, we refer to the EMC increases as increase events. The typical amplitude of EMC increase is tens of percent, but in some events it runs to 100 % of the level immediately before precipitation. The increases are observed during any precipitation events in liquid (rain, fog) or solid (snow, ice dust during severe frosts) form. The duration of the increases roughly corresponds to the duration of precipitation: after precipitation ceases, the radiation flux gradually returns to the previous level. The charged particles detectable by ground-based detectors are known to accelerate in strong electric fields of thunderclouds [de Mendonca et al., 2011; Mironychev, 2003; Muraki et al., 2004]. In addition, the effect of runaway electrons, which produce bremsstrahlung radiation, is observed [Gurevich et al., 1992; Gurevich, Milikh, 1999; Gurevich, Zybin, 2001]. During lightning discharge, X-ray radiation also occurs from high-temperature plasma in the lightning channel [Dwyer et al., 2003, 2004]. However, the above-mentioned effects of generation of X-rays and gamma radiation can occur only during thunderstorms, whereas the increases we have detected are observed in winter and summer in the polar regions, where thunderstorms are very rare, and only in the electromagnetic component. Deployment of identical detectors in other places (in the Svalbard archipelago, in the Caucasus, Tixie, etc.) has shown that the increases occur at all stations, although there are some features associated with the observation point. Figure 1 exemplifies such increases at the stations Apatity, Barentsburg (Svalbard archipelago), and Neutrino (North Caucasus). To identify the origin of the increases, additional experiments have been carried out [Germanenko et al., 2011]. The analysis of precipitation, collected during an increase event, carried out in the radiological laboratory has shown only trace amounts of radionuclides.

At the cosmic ray station in Apatity, a differential precipitation gauge, which measures the precipitation rate, was installed on the roof of the building [Shishaev, Beloglazov, 2011]. Its operation principle is based on measuring the IR radiation scattered by falling hydrometeors. The precipitation gauge is not calibrated; it is used for qualitative evaluation of precipitation.

Thorough analysis of the increase events and related circumstances has revealed that there is no addi-

tional release of radon caused by the effect of precipitation on soil permeability. Figure 2 exemplifies a typical EMC increase, which occurred on April 5, 2012. The daily average temperature in the latter half of March and in the first half of April did not rise above -10° C. According to [https://rp5.ru], the snow depth was ~ 80 cm; the snow was dense, packed for a long winter period. There was a layer of frozen soil under the snow cover. The April 05, 2012 increase event is associated with short snow squalls coming one after another. The differences between readings of the precipitation gauge are explained by the different form of precipitation during these snow squalls. The first squall brought precipitation in the form of snow pellets, which moderately dissipates IR radiation, and the second and third squalls brought precipitation in the form of large snowflakes. The amount of precipitation estimated from new snowfall was roughly the same. Each squall lasted for no more than half an hour, leaving a fresh snow layer of ~ 2 cm. If we suppose that the increase events are caused by enhanced radon release from soil during precipitation, a fundamental question arises as to how the small layer (~ 2 cm) of fresh loose snow that fell on top of the thick (~ 80 cm) layer of snow packed for months affects the rate of radon release from soil. The lower layers of the packed snow cover do not change their physical conditions in any way, nor does the frozen soil beneath them. It is such winter events that clearly show that the increases are unrelated to the additional radon release from soil.

Later, a charged particle detector (CPD) based on Geiger counters was added to the thermobox. The CPD effective area is 180 cm^2 , the estimated energy loss of a particle detected in the roof is taken to be $\sim 6 \text{ MeV}$ [Murzin, 1988]. The NaI crystal scintillation detector is effective at detecting both electromagnetic radiation and charged particles (electrons, positrons, and muons) [Abramov et al., 1985]. Geiger counters, on the contrary, have very low sensitivity to electromagnetic (X-ray and gamma) radiation [Abramov et al., 1985]. Comparison and analysis of SCR variations using these two detectors allow us to determine in which SCR components a variation occurs. The result is as follows. Firstly, the percentage of charged particles is lower than 10 % of the total flux through the NaI crystal, i.e. the scintillation detector counting rate is mainly determined not by charged

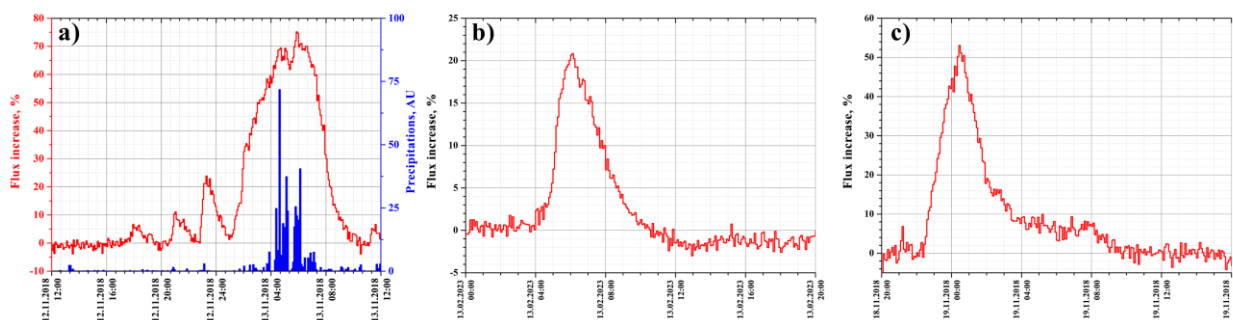


Figure 1. Profiles of electromagnetic radiation fluxes recorded at the stations Apatity (a), Neutrino (b), and Barentsburg (c). For Apatity, the amount of precipitation is also given in conventional units (a). Five-minute averaging is used; the raw data has minute resolution. The statistical measurement error is less than 1 % for the level before an increase

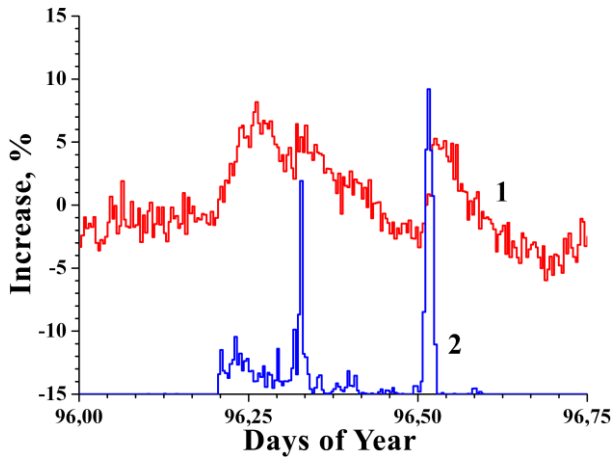


Figure 2. The April 05, 2012 increase event; >100 keV channel (curve 1). The amount of precipitation (curve 2) is given in relative units and shifted along the scale for convenience

particles, but by the electromagnetic radiation flux. Secondly, during precipitation there is no significant increase at CPD: even with a 50 % EMC increase, the possible increase in the counting rate does not exceed 3–4 %. Results of the study into increase events are reported in detail in [Germanenko et al., 2011; Balabin et al., 2014].

Observations of SCR EMC over the period 2010–2022 have revealed the following:

1. Precipitation-related EMC increases are observed at all observation stations: Barentsburg (Svalbard); Apatity; Tixie; Yakutsk; Mondy village, (Eastern Sayan), 2800 m; Rostov-on-Don; Neutrino (North Caucasus), 1700 m.

2. The EMC increases occur all year round, although during the cold period when precipitation falls in solid form, the amplitude of the increases decreases, on average, 1.5–2 times.

3. The increases are observed only in SCR EMC. During the increase events there is no noticeable increase in the flux of charged particles such as electrons, positrons, muons.

4. There are long-lived natural radionuclides in precipitation only in trace amounts.

5. In 2020, a scintillation detector was installed on board a scientific ship performing biological research in the Barents and Greenland Seas [Balabin et al., 2022]. For two weeks, the ship was in the open sea at a distance of hundreds of kilometers from the nearest land. Increase events with 15–25 % amplitude were recorded during precipitation.

As a result of long-term observations, it has been understood that the EMC increases are most likely unrelated to the presence of any radionuclides in precipitation, but are caused by some other factor that manifests itself in the atmosphere during precipitation. Confirming this requires direct spectral measurements of EMC.

2. MEASUREMENTS OF THE EMC DIFFERENTIAL SPECTRUM

Many research teams are engaged in measuring spectra of X-rays and gamma radiation coming from

the environment. First of all, this is done to monitor air, water, and soil pollution with radionuclides [Zorina et al., 2008; Petrova et al., 2009]. Radionuclide type and concentration are determined from known emission lines. In these works, attention is focused on radionuclide lines, and EMC present in the atmosphere serves as a background whose level in each case is taken as initial [Torii et al., 2002, 2009].

Other teams examine the effect of thunderstorm activity on SCRs, primarily on charged particle fluxes [Gurevich et al., 1992; Gurevich, Zybin, 2001; Dwyer et al., 2003, 2004; de Mendonca et al., 2011]. These works have been mentioned above. Such observations are carried out at stations in low and middle latitudes, where thunderstorm activity is significant. The result of theoretical calculations [Gurevich, Milikh, 1999] and numerous observations (e.g., [Alexeenko et al., 2002a; Alekseenko et al., 2002b; Lidvansky et al., 2004]) is the conclusion that charged particles can accelerate in strong electric fields of thunderclouds at an electric field strength of hundreds of kV/m, despite the high density of the atmosphere. When moving in such a dense medium as Earth's atmosphere, light charged particles will produce additional bremsstrahlung radiation [Heitler, 1936; Gurevich, Milikh, 1999]. Nonetheless, SCRs are usually not divided into electromagnetic and charged components during measurements, it is implied that thunderstorm activity has an effect on fluxes of SCR charged particles. Thunderstorms are extremely rare in polar regions, hence the results of these works cannot be applied to our observations.

In mid-2022, an EMC spectrometer was installed and put into continuous operation in Apatity. The spectrometer is comprised of a NaI(Tl) scintillation crystal 65 mm in diameter and 65 mm high and is housed in a thermobox close to other EMC detectors in the same cup made of lead bricks. The spectrometer's field of view is limited by walls of the cup and corresponds to a cone with an angle of $\sim 90^\circ$ whose base is oriented to the zenith. The energy range is 0.1–4 MeV; the time it gets to obtain one differential spectrum is 30 min. Of course, a longer time improves the accuracy of spectrum measurement and reduces fluctuations. However, since increase events often last for 2–3 hrs, it would be preferable to obtain several spectral measurements during this time in order to be able to select the spectra corresponding separately to the maximum phase or to the ascending phase. Based on these two conditions, a compromise value of 30 min was chosen. A high-speed 4096-channel amplitude pulse analyzer is used with the crystal, which provides measurement of the differential spectrum at a step of ~ 1 keV per channel for the selected energy range and gain settings. The spectrometer is calibrated against lines of several radionuclides: K-40, Na-22, Cs-137, Co-60. For the Cs-137 line (660 keV), the resolution was 5.1 %, which is slightly higher than indicated in the technical documentation — 5.7 %.

Using the RUSCOSMICS software package [Germanenko et al., 2019], the photon detection efficiency $Q(E)$ for this crystal was determined depending on the photon energy in the entire operating range. In calculations with the RUSCOSMICS package, we can specify not only the type of crystal and its dimensions, but also physical parameters of the spectrometer: material and dimensions of the protective shell. From tabular data [Grigoriev, Melikhov, 1991], photon absorption coefficients $\mu(E)$ in the roof material in the operating energy range were determined. Based on the derived dependences $Q(E)$ and $\mu(E)$, corrections are made to the spectral measurements so that finally the spectrum fits the primary radiation in the atmosphere near the roof. Hereinafter, we use the spectrum reduced to the primary radiation.

For six months (June–December 2022), we recorded 68 increase events with an amplitude of $>10\%$. Such a threshold for increase events is set as a reasonable lower limit: the calculated difference between spectra at a lower amplitude becomes comparable to the level of fluctuations, it is difficult to recognize any lines. Moreover, there are different variations in the electromagnetic radiation flux with an amplitude up to 5% . These low variations usually last for a day or longer; it is not possible to associate them with certain weather phenomena, their cause is unclear.

Figure 3 shows EMC spectra in the July 14, 2022 increase event. The increase profile is constructed according to the data from the >100 keV channel of the integral detector based on the NaI(Tl) crystal. Further in the work, where the increase profiles and amplitudes are discussed, we mean the data from the integral detector installed near the spectrometer. To calculate the average spectrum before an increase, ten spectra recorded from 5 to 10 UT have been used (the interval is indicated by segment 1 on the profile). This average spectrum is called basic. At the increase maximum from 11 to 12 UT, indicated by segment 2 in Figure 3, *a*, two spectra were detected. The resulting average spectrum is called the increase spectrum for short. Figure 3, *b* exhibits the

average spectra for given intervals 1 and 2, as well as their difference. By subtracting the basic spectrum from the increase spectrum, we obtain the spectrum of the additional radiation itself, which caused the increase effect. Let us call it the additional-flux spectrum (AFS). Each event therefore incorporates spectra of the following three groups: 1) a set of basic spectra; 2) a set of increase spectra (sometimes there are only 2–3 of them); these two sets yield the average basic spectrum and the average increase spectrum; 3) AFS obtained as the difference of the first two. It is easy to obtain the average basic spectrum with high accuracy since there is usually a sufficient time interval with a stable electromagnetic radiation flux before the increase. The increase spectrum corresponding to the maximum of the event is obtained with lower accuracy since the maximum period of the event is usually 1–2 hrs, rarely longer. From the increase profile shown in Figure 3, *a* it is clear that to compare the spectra we should choose an interval in the vicinity of the maximum, where, first, the obtained increase spectrum matches a relatively stable radiation flux, and second, the difference between the spectra will be the greatest and the accuracy will be higher. During the ascending and descending phases for the time when one spectrum is being constructed, the radiation flux changes significantly, and such a spectrum proves to be too rough approximation. In what follows, the increase spectrum for each event means the spectrum at the maximum of the event.

The basic spectrum has a small number of separate lines against the background of the continuous component. The 511 keV line (An in Figures 3 and 4) is noticeable which corresponds to annihilation of positrons in the atmosphere. Positrons are formed in the atmosphere as one of SCR components [Murzin, 1988]. The annihilation cross-section of positrons is inversely proportional to their velocity [Heitler, 1936]; therefore, the vast majority of energetic positrons annihilate only after they lose their energy. For this reason, the annihilation peak corresponds to the positron rest energy.

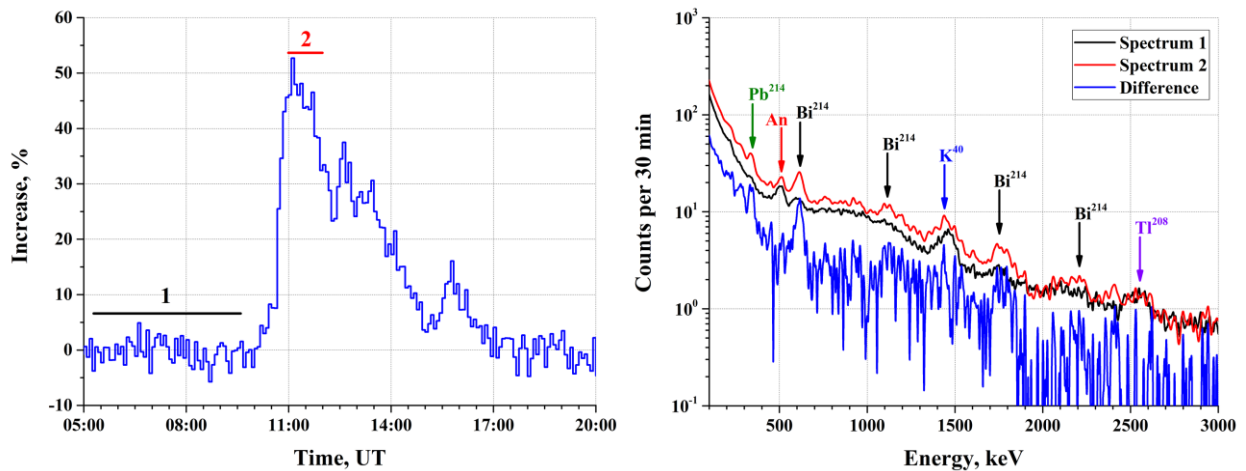


Figure 3. At the left is the July 14, 22 EMC increase profile as recorded by the integral detector in the >100 keV channel; segments 1 and 2 mark the intervals when EMC differential spectra were obtained. At the right: spectrum 1 is the average EMC spectrum before an increase (basic), spectrum 2 is the average spectrum at a maximum increase; the difference is AFS derived from them

The pronounced 1460 keV line is peculiar to the decay of K-40. Gamma radiation is not emitted during β decay of the K-40 nucleus [Grigoriev, Melikhov, 1991; Iskra, Bakhurov, 1981]. Nonetheless, with a probability of 10 %, K-40 decays through electronic capture, which leads to the formation of an excited Ar-40 nucleus whose lifetime is picoseconds; then the Ar-40 nucleus goes to the basic level, emitting a 1460 keV quantum [Grigoriev, Melikhov, 1991]. This line is an indicator of the K-40 decay. Weak lines Bi-214 (609 and 1764 keV [Grigoriev, Melikhov, 1991]) and Tl-208 (2614 keV [Lee, 2017]) can also be seen in the basic spectrum. There are no other noticeable lines in the basic spectrum.

K-40 is a natural radionuclide with a long half-life period. The presence of the K-40 line in the basic spectrum is natural because potassium is present in living organisms, in wood, and is also part of many common minerals: silicates, feldspars, etc. The radionuclide Bi-214 is a daughter nuclide of U-238, and Tl-208 is a daughter nuclide of Th-232 [Kozlov, 1991]. U-238 and Th-232 are radionuclides present in most rocks, so the presence of these lines in the spectrum is natural.

In the increase spectrum, the lines already present in the basic spectrum intensify, and the Pb-214 (352 keV) and Bi-214 (1120 keV, 1764 keV) lines appear. The weak line of ~2200 keV presumably also belongs to Bi-214 [Lee, 2017], but it is omitted in our further calculations. In general, as can be seen in Figure 3, both spectra are continuous incident with separate lines.

The most interesting is the AFS derived by subtracting the basic spectrum from the increase spectrum. Note that all the obtained differential spectra are arrays containing the number of photons in the energy range $[E, E+dE]$, where $dE=1$ keV, and E takes integer values from 100 to 4000 keV. Element-by-element subtraction of the basic spectrum from the increase spectrum yields AFS. Despite the significant amplitude of the increase, the accuracy of the obtained single AFS is low. Figure 4 presents the result of summing the spectra of nine events with an amplitude over 20 %. The basic spectrum has been obtained by averaging nine basic spectra of selected events. The increase spectrum of these nine events has been derived in the same way. AFS in Figure 4, obtained as a difference between these two spectra, has much higher accuracy, and some important features are clearly visible in it.

Qualitative analysis of the spectra in Figure 4 shows that all the three spectra are similar in shape, and the radionuclide lines are weak and do not determine the shape of the spectra. The shape of the spectra is determined by the continuum part described by a decreasing function. The increase spectrum is in fact the basic spectrum multiplied by a certain value, accordingly the AFS calculated as their difference is also similar to the basic spectrum. This implies that the radiation does not originate from radionuclides.

The first thing that draws attention: there is no annihilation line in AFS! Consequently, the positron flux at the ground level does not change during an increase event, the positron annihilation rate remains the same.

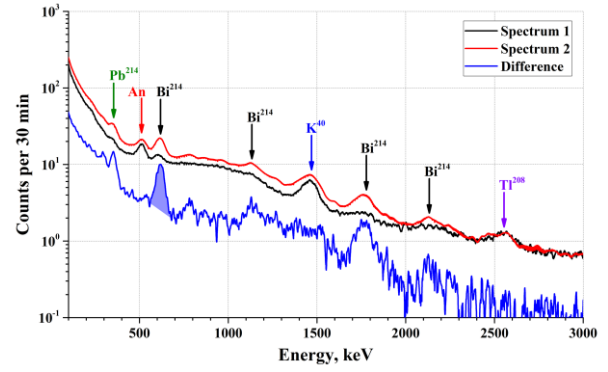


Figure 4. EMC spectra averaged over nine increase events with an amplitude over 20 %. Events for the warm period of the second half of 2022 were used.

Second, there are no K-40 and Tl-208 lines in AFS either. This means that sources of these lines are located in the surrounding objects and are not associated with precipitation, their corresponding contributions to the spectra are the same, when subtracted they are zero. The Pb-214 and Bi-214 lines stand out in AFS, and the weak lines in Figure 3 are well manifested in Figure 4. A very weak line of ~760 keV may belong to Bi-214 [Lee, 2017].

The upper energy threshold of the increase effect is determined from AFS. Figure 4 shows that near 2500 keV AFS reflects only random fluctuations of the initial spectra from which it has been derived. Thus, the previously obtained estimate of the upper threshold proved to be correct. The spectrum of the additional flux that causes an increase has the upper threshold of 2500 keV.

Figure 4 more clearly illustrates the procedures that are performed on AFS in all events. First, the spectral function integral in the operating energy range is calculated:

$$N = \int_{E_{\min}}^{E_{\max}} S_{\text{ad}}(E) dE, \quad (1)$$

where E_{\max} and E_{\min} are the upper and lower energy thresholds for the spectrometer (recall that these are 100 and 4000 keV); $S_{\text{ad}}(E)$ is the additional-radiation spectrum. N is the number of additional photons that caused an increase.

Second, the spectral function integral with weights for the same interval is calculated:

$$F = \int_{E_{\min}}^{E_{\max}} S_{\text{ad}}(E) E dE. \quad (2)$$

F is the energy contributed by N photons of the additional flux. Since all the spectra are one-dimensional arrays, Expression (1) represents the summation of the array elements; and (2), the summation with weight.

Note that AFS as a whole is also a continuous spectrum with separate lines of elements, and only small fluctuations are observed in wide bands (for example, 400–550 keV, 800–1050 keV). Since the lines are well separated, we can estimate the partial contributions of photons of each radionuclide line present in the spectrum: Pb-214 (352 keV), Bi-214 (609, 1120, and 1764 keV), etc.

As an example, Figure 4 shows the partial contribution of photons of the 609 keV line by filling the “bell” of this line. The base of the “bell” is the interpolation between the spectral regions before and after the selected line. The partial contribution is calculated from Expression (1) within the line width:

$$N_i = \int_{E_{i,1}}^{E_{i,2}} (S_{\text{ad}}(E) - Z_i(E)) \cdot dE, \quad (3)$$

where $E_{i,1}$ and $E_{i,2}$ are the left and right energy limits of the line i ; $Z_i(E)$ is a function interpolating in a bounded spectral region without taking into account this radionuclide line; N_i is the number of photons emitted by radionuclide in the i line.

It will also be useful to determine the photon energy averaged over the spectrum or any its region calculated from the formula:

$$\varepsilon = \frac{\int_{E_{\text{min}}}^{E_{\text{max}}} S(E) E dE}{\int_{E_{\text{min}}}^{E_{\text{max}}} S(E) dE}, \quad (4)$$

where $S(E)$ is one of three available spectra. Substituting the basic spectrum into the formula yields the average photon energy of the background; substituting AFS, the average photon energy of the additional flux. The average photon energy calculated from any spectrum is an integral characteristic reflecting the contribution of

different energies in the spectrum. A harder spectrum as a whole or the addition of high-energy photons will provide a higher average energy.

Special programs have been developed to perform the described procedures with spectra of all recorded increase events. The spectra were processed by a single algorithm, an operator only chose intervals 1 and 2 (see Figure 3) and set $E_{i,1}$ and $E_{i,2}$. We have used 68 increase events $>10\%$. The results are presented in Figure 5.

Figure 5, *a* shows the dependence of the total energy, supplied by photons of additional radiation, on the increase amplitude. There is a clear linear dependence, especially if it is plotted over lower values.

The number of photons in the 352, 609, and 1764 keV lines also shows a linear dependence on the increase amplitude. Absence of the annihilation line dependence on the amplitude means that precipitation does not affect this SCR component. The same applies to the K-40 line. This conclusion has already been made earlier when analyzing AFS; in this paper, it is independently confirmed. Consequently, in the future these two lines will not be taken into account when calculating the contributions. Note that more than 2/3 of the events have an increase amplitude of $<20\%$. With decreasing amplitude, the spread of values increases markedly. The wide spread at lower amplitudes is most likely caused by the contribution of small (to 5%) variations,

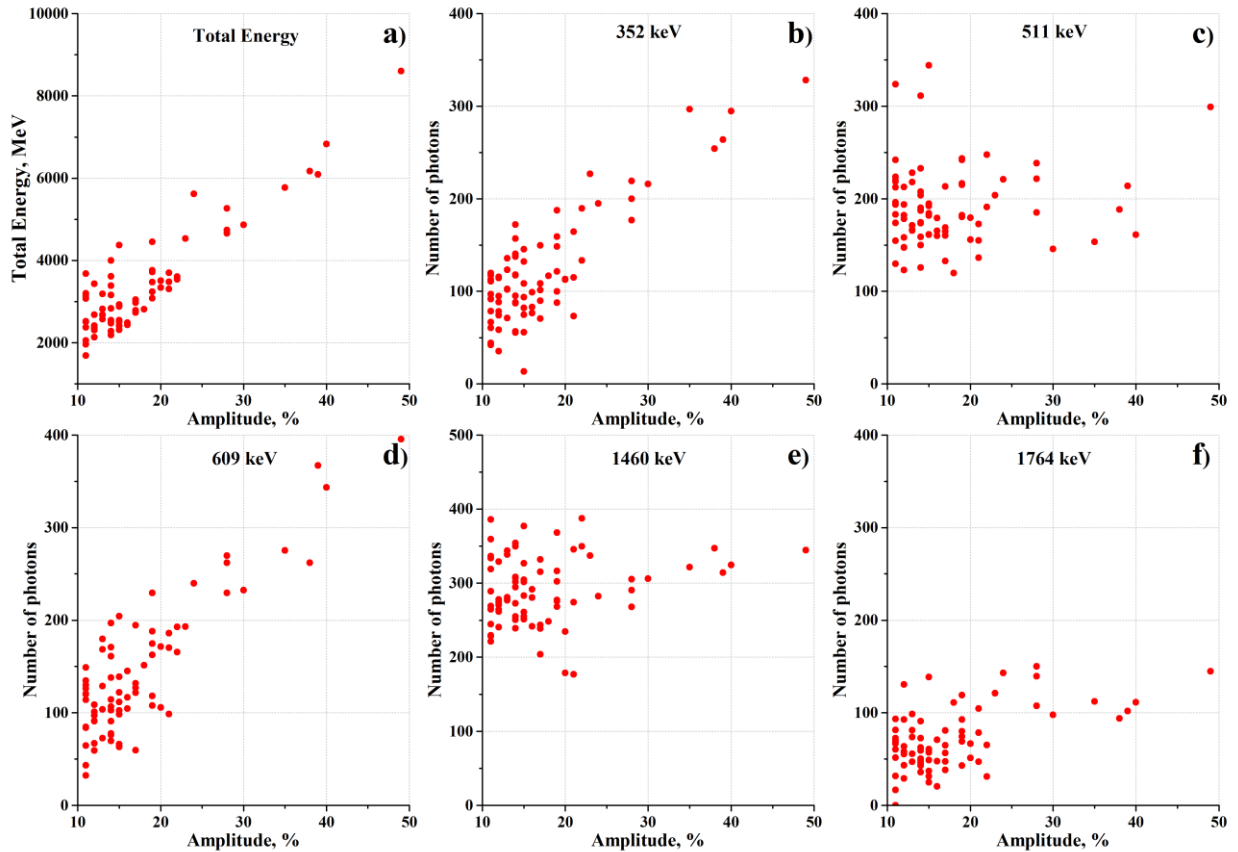


Figure 5. Results of processing of the array of spectra obtained in increase events in 2022: *a* — the total energy provided by additional radiation, calculated from (2); *b–d* — the number of photons emitted in the 352 keV (Pb-214), 511 keV (annihilation peak), 609 keV (Bi-214), 1460 keV (K-40), and 1764 keV (Bi-214) lines. One point of the plot is one increase event and one AFS from which these values are obtained

which have been mentioned above and are not related to precipitation. Superimposed on increases in precipitation, these variations introduce an additional error and lead to a spread of calculated values at lower amplitudes. With a rise in the increase amplitude due to precipitation, the role of other variations decreases, and the events with $>20\%$ amplitude form linear dependencies much more clearly. It seems convenient to switch to the normalized values obtained by processing the spectra. Normalization should be done to the increase amplitude, which will more clearly indicate a contributor.

Since the number of photons emitted by radionuclides in different lines and received by the spectrometer is known, it is easy to calculate the total energy provided by these photons. In total, lines with energies of 352, 609, 764, 1120, and 1764 keV have been detected in AFS in dozens of events. Having determined the number of photons for each line from Expression (3), we estimated the total energy contributed by these lines to AFS. The results are presented in Figure 6.

DISCUSSION

Figure 6, *a* is Figure 5, *a* in normalized form. Figure 6, *a* clearly illustrates the constancy of the specific energy release: during an increase, $\sim 170\text{--}180$ MeV per 1% of amplitude is additionally supplied to the crystal. This is especially evident for $>20\%$ amplitudes. Figure 6, *b* characterizes the specific total energy received from all radionuclide lines present in AFS. Similarly, the constancy of the energy transferred by radionuclides is ob-

served: $\sim 17\text{--}8$ MeV per 1% of amplitude.

Figures 5 and 6, *a, b* indicate that the increase amplitude and the number of radionuclides are linearly related. This seems to suggest that radionuclides are the main cause of the increase. This is contradicted by the data, presented in Figure 6, *c, d*, and by the ratio of total energies. To ensure the observed increase amplitude, the energy flux must be an order of magnitude greater than all the radionuclide lines present in AFS can provide.

Figure 6, *d* exhibits the average photon energy of the background ε_b calculated from the average basic spectrum from (4). Values of ε_b remain around 0.45 MeV for the entire set of events. This is confirmed by measurements with the integral detector: during the entire period of spectrum measurements, the background electromagnetic radiation flux changed little; after any increase, the electromagnetic radiation flux came to the previous level. Figure 6, *c* displays the average photon energy with increasing ε_I , calculated from AFS. The spread of ε_I values is wider than the spread of ε_b , but ε_I also has a value of ~ 0.45 MeV. The proximity of ε_I and ε_b means that the basic spectrum and AFS differ little in shape. The value of 0.45 MeV is lower than the energies of the radionuclide lines listed above in AFS, except for the 352 keV line, hence a significant contribution of these lines would lead to an increase in ε_I . The proximity of average energies at all increase amplitudes, even at the highest ones, confirms that the contribution of radionuclide lines to the spectrum and hence to the increase is small.

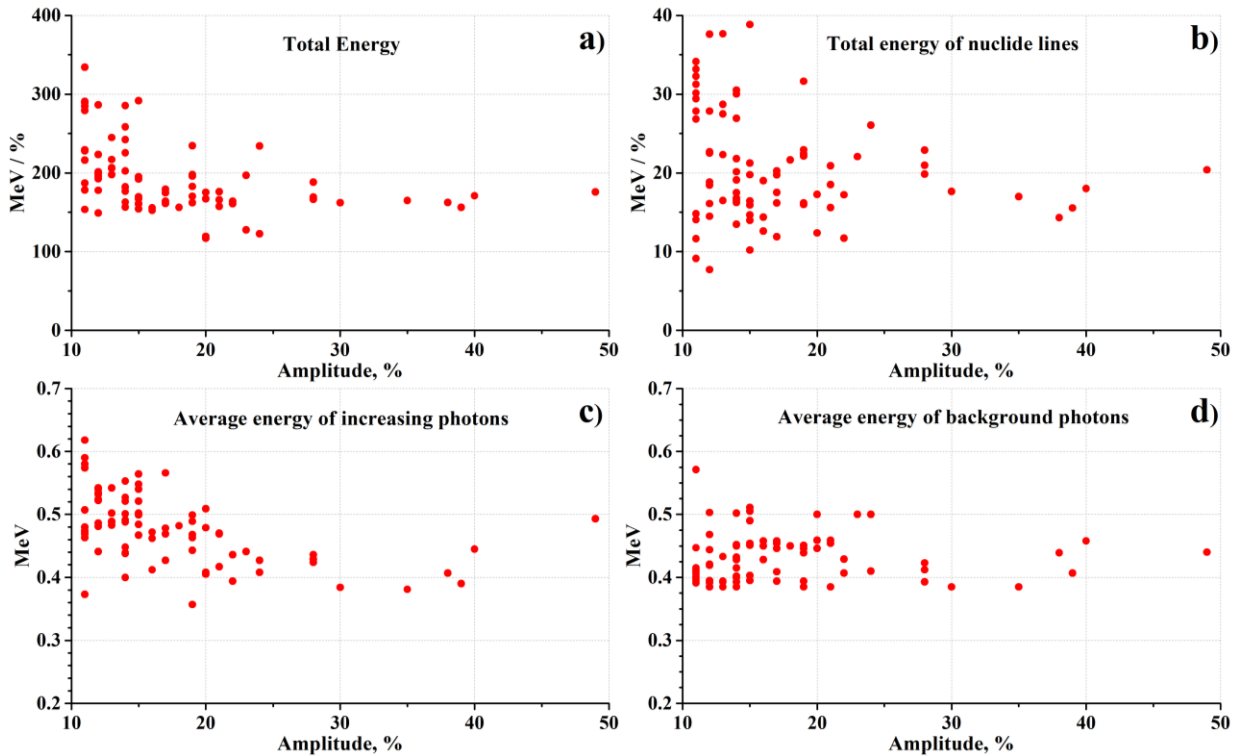


Figure 6. Total energy (*a*) with additional radiation, and total energy (*b*) contributed by radionuclide lines, normalized to 1% of increase amplitude; average photon energy during an increase event (*c*); average photon energy of the background (*d*). One point of the plot corresponds to one event and one AFS, from which these values have been obtained

Another evidence for the insignificance of the influence of radionuclide lines during an increase event is given in Figure 7. On February 21, 2023, an increase event with 20 % amplitude was detected. The peculiarity of this event was its long duration. For more than half a day, the increase amplitude was at the level 18–20%, this period corresponded to prolonged bad weather with a blizzard and snowfall. This made it possible to obtain AFS for a single event with adequate accuracy. For comparison, we have taken six ordinary events observed in December 2022. It has been mentioned earlier that events in different seasons have on average different increase amplitudes; accordingly, events of close amplitude for one season should be taken for comparison. November 2022 could not yet be called a truly winter month, it was warm, there were rains, a stable snow cover formed in the latter half of the month. Therefore, for comparison, we took the December events when the temperature was constantly negative and a constant snow cover was formed. These events had an amplitude 18–21 %, the maximum duration of each was 1–2 hrs. We got average AFS for these six events. Figure 7 shows two AFS — for six December events and for a single event in February. On the left panel, for clarity, the spectral regions are presented in a linear scale.

These two increase events (averaged December one and the single event in February) have a close amplitude, close in absolute AFS. The events occurred during the cold season, accompanied by precipitation of one type — snow. During winter events, as inferred from spectral measurements, the radionuclide lines are less pronounced, but, as can be seen from December AFS, the 609 keV line is quite clear, other lines hardly stand out against the background of fluctuations. The December AFS is similar to the spectra for the rest of the winter events. There are practically no lines in the February ASF, the strongest 609 keV line is scarcely seen, yet this AFS corresponds to the event with the same 20 % increase amplitude.

Note that long before the spectral measurements, the authors were convinced of the small contribution of radio-

nuclides to the observed effect of precipitation-related EMC increase after a visual experiment. The experiment was as follows. During a heavy summer rain, when the working detector showed an increase similar to that shown in Figure 3, *a*, rainwater of volume 5 l from the roof of the building was collected in a plastic bottle. According to the estimates based on [Matveev, 1984], the weight of water in the bottle matched the weight of the drops that were in the field of view of the working detector up to 80–100 m. No more than 5 min after collection, the bottle of water was placed on an additional detector inside the protection, made of lead bricks and covering the detector from all sides. The detector was identical to that used for observations. The additional detector with rainwater on it did not notice any increase, while the working detector, in whose field of view there was almost the same amount of water in the form of raindrops, showed a 40–50 % increase!

This experiment found a significant but indirect evidence that there are no many radionuclides in precipitation. More accurate and convincing results allowed spectral measurements to be made.

Lee [2017] used a spectrometer for spectral observations similar to that we applied, with similar characteristics. It was installed in a campus of the Korean University, and for about a year it was used to monitor X-ray and gamma radiation. The main purpose of the monitoring was to measure composition and concentration of radionuclides in the environment. The author points to the fact that the gamma radiation flux increases during precipitation. Figure 5 given in [Lee, 2017] clearly traces the precipitation-related increase events, but the author focused on radionuclide lines and calculation of the dose that these radionuclides provide, ignoring variations in the background level.

In Figure 8, we present a scan of Figure 10 from [Lee, 2017]. A similar effect is clearly seen: the spectrum during precipitation (orange) is similar to the background spectrum (blue), shifted to larger values. Lee [2017] does not comment on this fact in any way and does not note it, it does not matter to him. Figure 8 also clearly shows that

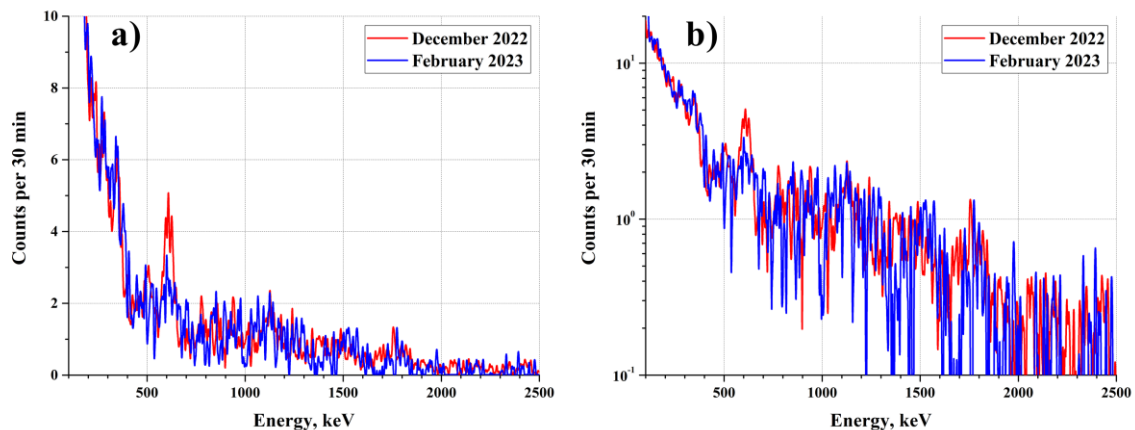


Figure 7. AFS for winter events: *a* — spectral regions on a linear scale to show a significant 609 keV line; *b* — the entire spectrum on a semi-logarithmic scale. AFS indicated by the red line is averaged over six increase events on December 21–25, 2022.

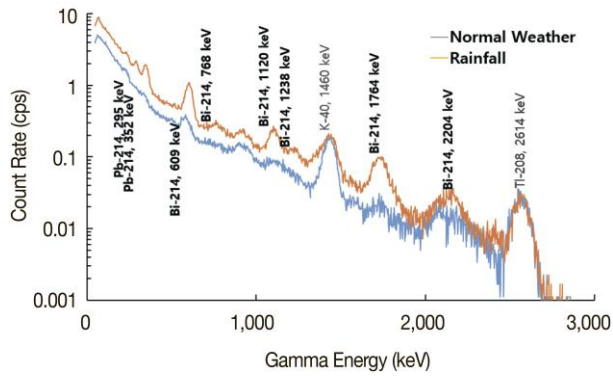


Figure 8. Measurements of EMC spectrum during precipitation. The observations were carried out near Seoul (Korea). The Figure has been taken from [Lee, 2017], where you can also find detailed information about the spectrometer employed and a summary table with dozens of similar events

both spectra ~ 2500 keV begin to coincide, which indicates the upper energy threshold of AFS near 2.5 MeV. We have made the same estimate of the upper energy threshold of AFS in [Balabin et al., 2014]. Here, the upper threshold is obtained from direct measurements of the differential spectrum.

The spectra in Figure 8 were digitized, and a basic spectrum and an increase spectrum were obtained as arrays allowing AFS to be calculated for this event detected in Korea. The integral characteristics of the increase were also calculated. The spectra in Figure 8 correspond to ~ 80 % EMC increase; the contribution of all radionuclides present in the line spectrum was 0.12 of the total energy provided during the increase. The mean energy of the spectrum $\varepsilon_l = 0.47$ MeV. As we can see, the characteristics of the event given in [Lee, 2017] as a typical example are close to those that we have obtained for EMC increases in Apatity.

Other works have also obtained the evidence of EMC increases during precipitation. For example, Torii et al. [2009] in Figure 1 indicate that the counting rate of a detector increases during a thunderstorm, but the authors examine only the effect of short increases caused by lightnings. This suggests that the effect of increasing the counting rate of a detector during precipitation has also been observed in measurements by other research teams studying gamma radiation variations in the atmosphere; however, since they have other research goals, variations in the background radiation are ignored.

Main results of spectrometric measurements

1. The basic spectrum measured before an increase, the increase spectrum measured at the maximum of the event, and their AFS difference are similar. They represent a continuous decreasing function with separate radionuclide lines, few and moderate in intensity.

2. The total energy provided by all the radionuclide lines is an order of magnitude lower than the total energy received by the detector during the same period during an increase event.

3. Among winter increases with ~ 20 % amplitude, there are events whose AFS has practically no pronounced radionuclide lines.

4. The average energies calculated from the basic spectrum and AFS differ slightly. The average energies are ~ 0.45 MeV. The radionuclide lines, except one, have energy significantly higher than the average energy. If the contribution of the lines were significant, this would lead to a shift in the average energy toward larger values.

As a result of long-term measurements of differential EMC spectra during periods of good weather and during precipitation, it can be considered established that the observed increases in the electromagnetic radiation flux are not due to the presence of radionuclides in precipitation. Apparently, these increases result from changes in conditions of SCR propagation and interaction in the atmosphere, which were caused by meteorological processes. To find the cause for the precipitation-related increase in electromagnetic radiation fluxes, further detection of EMC spectra in different geographical locations is required.

CONCLUSION

Monitoring of the electromagnetic component (EMC) of secondary cosmic rays arising in the atmosphere has been carried out at the Polar Geophysical Institute for more than ten years at a number of stations: Barentsburg (Svalbard archipelago), Apatity (Kola Peninsula), Rostov-on-Don, Neutrino (North Caucasus), Mondy village (Eastern Sayan). Numerous (dozens per year) increase events in the electromagnetic radiation flux by 10–50 % or more were observed at all the observation stations. In most cases, these events were accompanied by precipitation. Additional experiments indirectly indicate that radionuclides cannot cause an increase. In 2022, continuous measurements of the differential spectrum of electromagnetic radiation in the range 0.1–4 MeV were started in Apatity using a NaI(Tl) spectrometric crystal and a 30 min construction time of one spectrum. EMC spectra have been obtained at a maximum of 68 increase events. The spectra before an increase and during the period of maximum increase amplitude have a similar shape: an incident continuous spectrum with separate radionuclide lines of low intensity. A method has been developed for obtaining a spectrum of additional radiation that causes an increase. These spectra have been thoroughly analyzed. Lines of some radionuclides are present in all the spectra. The most pronounced among them are K-40, Pb-214, Bi-214. However, the total fraction (by the number of quanta) of all radionuclide lines is ~ 0.1 of the flux that caused the increase. In one of the winter events with an increase amplitude of ~ 20 %, the spectrum had radionuclide lines barely distinguishable against the background of fluctuations, there were practically no radionuclide lines. Accordingly, it can be considered established that the effect of EMC increase during precipitation is not caused by radionuclides in precipitation. The EMC increases are of a different nature and, apparently, are caused by the influence of meteorological processes in the atmosphere on propagation of secondary cosmic rays.

The work was financially supported by the Russian Science Foundation (Grant No. 18-77-10018).

REFERENCES

- Abramov A.I., Kazanskii Yu.A., Matushevich E.S. *Osnovy eksperimental'nykh metodov yadernoi fiziki* [Fundamentals of Experimental Methods of Nuclear Physics]. Moscow, Jenergoizdat Publ., 1985, 267 p. (In Russian).
- Alexeenko V.V., Khaerdinov N.S., Lidvansky A.S., Petkov V.B. Transient variations of secondary cosmic rays due to atmospheric electric field and evidence for pre-lightning particle acceleration. *Phys. Lett. A*. 2002a, vol. 301, iss. 3-4, pp. 299–306. DOI: [10.1016/S0375-9601\(02\)00981-7](https://doi.org/10.1016/S0375-9601(02)00981-7).
- Alekseenko V.V., Lidvansky A.S., Petkov V.B., Haerdinov N.S. About different types of increase in space rays before lightning categories. *Izvestiya RAN. Seriya fizicheskaya* [Bulletin of the Russian Academy of Sciences: Physics]. 2002b, vol. 66, no. 11, pp. 1581–1584. (In Russian).
- Balabin V.V., Germanenko A.V., Gvozdevsky B.B., Vashenyuk E.V. Variations in the natural X-ray background in the polar atmosphere. *Geomagnetism and Aeronomy*. 2014, vol. 54, no. 3, pp. 347–356. DOI: [10.1134/S0016793214020029](https://doi.org/10.1134/S0016793214020029).
- Balabin Y.V., Germanenko A.V., Mikhalko E.A., Maurchev E.A., Larchenko A.V. Observing variations in secondary cosmic ray fluxes during a sea expedition in the Arctic Ocean. *Bulletin of the Russian Academy of Sciences: Physics*. 2022, vol. 86, no. 3, pp. 285–289. DOI: [10.3103/S1062873822030030](https://doi.org/10.3103/S1062873822030030).
- de Mendonca R.R.S., Raulin J.-P., Bertoni F.C.P., Echer E., Makhmutov V.S., Fernandez G. Long-term and transient time variation of cosmic ray fluxes detected in Argentina by CARPET cosmic ray detector. *J. Atmos. Solar-Terr. Phys.* 2011, vol. 73, iss. 11-12, pp. 1410–1416. DOI: [10.1016/j.jastp.2010.09.034](https://doi.org/10.1016/j.jastp.2010.09.034).
- Dorman L.I. *Meteorologicheskie efekty kosmicheskikh luchei* [Meteorological Effects of Cosmic Rays]. Moscow, Nauka Publ., 1972, 212 p. (In Russian).
- Dorman L.I. *Eksperimental'nye i teoreticheskie osnovy astrofiziki kosmicheskikh luchei* [Experimental and Theoretical Foundations of Astrophysics of Cosmic Rays]. Moscow, Nauka Publ., 1975, 402 p. (In Russian).
- Dwyer J.R., Rassoul H.K., Al-Dayeh M., Caraway L., Wright B., Chrest A., Uman M.A., et al. A ground level gamma-ray burst observed in association with rocket-triggered lightning. *Geophys. Res. Lett.* 2004, vol. 31, iss. 5, L05119. DOI: [10.1029/2003GL018771](https://doi.org/10.1029/2003GL018771).
- Dwyer J.R., Uman M.A., Rassoul H.K., Al-Dayeh M., Caraway L., Jerauld J., Rakov V.A., et al. Energetic radiation produced during rocket-triggered lightning. *Science*. 2003, vol. 299, no. 5607, pp. 694–697. DOI: [10.1126/science.1078940](https://doi.org/10.1126/science.1078940).
- Germanenko A.V., Balabin Yu.V., Vashenyuk E.V., Gvozdevsky B.B., Schur L.I. High-energy photons connected to atmospheric precipitations. *Astrophys. Space Sci. Trans.* 2011, vol. 7, iss. 4, pp. 471–475. DOI: [10.5194/astra-7-471-2011](https://doi.org/10.5194/astra-7-471-2011).
- Germanenko A.V., Maurchev E.A., Balabin Yu.V. Calculation of registration efficiency functions of NaI (Tl) scintillation detectors and comparison of model operation with real experiment data. *Trudy Kol'skogo nauchnogo tsentra RAN* [Proceedings of the Kola Scientific Center of the Russian Academy of Sciences]. 2019, vol. 10, no. 8-5, pp. 82–87. (In Russian). DOI: [10.25702/KSC.2307-5252.2019.10.8.82-87](https://doi.org/10.25702/KSC.2307-5252.2019.10.8.82-87).
- Grigoryev I.S., Melikhov E.Z. *Fizicheskie velichiny. Spravochnik* [Physical Quantities. Reference book]. Moscow, Energoatomizdat Publ., 1991, 1231 p. (In Russian).
- Gurevich A.V., Milikh G.M. Generation of X-rays due to multiple runaway breakdown inside thunderclouds. *Phys. Lett. A*. 1999, vol. 262, iss. 6, pp. 457–463. DOI: [10.1016/S0375-9601\(99\)00695-7](https://doi.org/10.1016/S0375-9601(99)00695-7).
- Gurevich A.V., Zybin K.P. Runaway breakdown and electric discharges in thunderstorms. *Physics–Uspekhi*. 2001, vol. 44, no. 11, p. 1119. DOI: [10.1070/PU2001v044n11ABEH000939](https://doi.org/10.1070/PU2001v044n11ABEH000939).
- Gurevich A.V., Milikh G.M., Roussel-Dupre R. Runaway electron mechanism of air breakdown and preconditioning during a thunderstorm. *Phys. Lett. A*. 1992, vol. 165, iss. 5-6, pp. 463–468. DOI: [10.1016/0375-9601\(92\)90348-P](https://doi.org/10.1016/0375-9601(92)90348-P).
- Hayakawa S. *Cosmic Ray Physics: Nuclear and Astrophysical Aspects*. New York, Wiley Interscience Publ., 1969, 774 p.
- Heitler W. *The Quantum Theory of Radiation*. Oxford, Clarendon Press, 1936, 252 p.
- Iskra A.A., Bakhurov V.G. *Estestvennye radionuklidy v biosfere* [Natural Radionuclides in the Biosphere]. Moscow, Jenergoatomizdat Publ., 1981, 123 p. (In Russian).
- Ivanenko I.P. *Elektromagnitnye kaskadnye protsessy* [Electromagnetic Cascade Processes]. Moscow, Moscow State University Publ., 1972, 176 p. (In Russian).
- Kozlov V.F. *Spravochnik po radiatsionnoi bezopasnosti. 4 izdanie* [Radiation Safety Handbook. 4th edition], Moscow, Jenergoatomizdat Publ. 1991, 352 p. (In Russian).
- Lazutin L.L. *Rentgenovskoe izluchenie avroral'nykh elektronov i dinamika magnitosfery* [X-ray Emission of Auroral Electrons and Dynamics of the Magnetosphere]. Leningrad, Nauka Publ., 1979, 200 p. (In Russian).
- Lee M.S. Gamma-ray Exposure Rate Monitoring by EnergySpectra of NaI (Tl) Scintillation detectors. *Journal of Radiation Protection and Research*. vol. 42, iss. 3, pp. 158–165. DOI: [10.14407/jrpr.2017.42.3.158](https://doi.org/10.14407/jrpr.2017.42.3.158).
- Lidvansky A.S., Petkov V.B., Haerdinov N.S. Cosmic ray muon intensity variations caused by thunderstorm electric fields. *Izvestiya RAN. Seriya fizicheskaya* [Bulletin of the Russian Academy of Sciences: Physics]. 2004, vol. 68, no. 11, pp. 1605–1607. (In Russian).
- Matveev L.T. *Kurs obshchei meteorologii* [The Course of General Meteorology]. Leningrad, Gidrometeoizdat Publ., 1984, 752 p. (In Russian).
- Mironychev P.V. Cosmic muons in thunderstorm electric fields. *Geomagnetism and Aeronomy*. 2003, vol. 43, no. 5, pp. 654–659.
- Muraki Y., Axford W.I., Matsubara Y., Masuda K., Miyamoto Y., Menjyou H., Sakakibara S., et al. Effects of atmospheric electric fields on cosmic rays. *Phys. Rev.* 2004, vol. 69, 123010. DOI: [10.1103/PhysRevD.69.123010](https://doi.org/10.1103/PhysRevD.69.123010).
- Murzin V.S. *Vvedenie v fiziku kosmicheskikh luchei* [Introduction to the Physics of Cosmic Rays]. Moscow, MSU Publ., 1988, 320 p. (In Russian).
- Petrova T.B., Miklyayev P.S., Vlasov V.K., Afinogenov A.M., Kirjukhin O.V. Variations in the content of ⁷Be in a ground layer of the middle latitude atmosphere. *Vestnik Moskovskogo universiteta. Seriya 2. Himiya* [Bulletin of Moscow University. Series 2. Chemistry]. 2009, vol. 50, no. 5, pp. 396–401. (In Russian).
- Shishayev V.A., Beloglazov M.I. Automatic recorder of atmospheric precipitation. *Pribory i tehnika eksperimenta* [Instruments and Technique of Experiment]. 2011, no. 2, pp. 156–158. (In Russian).
- Torii T., Sugita T., Tanabe S., Kimura Y., Kamogawa M., Yajim K., Yasuda H. Gradual increase of energetic radiation associated with thunderstorm activity at the top of Mt. Fuji. *Geophys. Res. Lett.* 2009, vol. 36, iss. 13, L13804. DOI: [10.1029/2008GL037105](https://doi.org/10.1029/2008GL037105).
- Torii T., Takeishi M., Hosono T. Observation of gamma-ray dose increase associated with winter thunderstorm and lightning activity. *J. Geophys. Res.* 2002, vol. 107, no. D17, p. 4324. DOI: [10.1029/2001jd000938](https://doi.org/10.1029/2001jd000938).
- Zorina L.V., Buraeva E.A., Davydov M.G., Stasov V.V. Radionuclide ²¹⁰Pb in atmospheric aerosols in a ground layer of air and meteorological parameters of Rostov-on-Don. *Izvestiya vuzov. Severo-Kavkazskii region. Seriya: Estestvennye nauki* [Bulletin of Higher Educational Institutions. North Caucasus Region. Natural Sciences]. 2008, no. 5, pp. 108–113. (In Russian). URL: <https://rp5.ru> (accessed February 22, 2023).

Original Russian version: Balabin Yu.V., Germanenko A.V., Gvozdevsky B.B., Mauricev E.A., Michalko E.A., published in *Solnechno-zemnaya fizika*. 2023. Vol. 9. Iss. 2. P. 41–51. DOI: [10.12737/szf-92202305](https://doi.org/10.12737/szf-92202305). © 2023 INFRA-M Academic Publishing House (Nauchno-Izdatelskii Tsentr INFRA-M)

How to cite this article

Balabin Yu.V., Germanenko A.V., Gvozdevsky B.B., Mauricev E.A., Michalko E.A. Precipitation-related increase events of the electromagnetic component of secondary cosmic rays: Spectral analysis. *Solar-Terrestrial Physics*. 2023. Vol. 9. Iss. 2. P. 37–47. DOI: [10.12737/stp-92202305](https://doi.org/10.12737/stp-92202305).